X-ray standing wave analysis of overlayer-induced substrate relaxation: The clean and Bi-covered (110) GaP surface

A. Herrera-Gomez
CINVESTAV-Querétaro, Querétaro, Querétaro 76010, Mexico

J. C. Woicik
National Institute of Standards and Technology, Gaithersburg, Maryland 20899, USA

T. Kendelewicz
Department of Geological and Environmental Sciences, Stanford University, Stanford, California 94305, USA

K. E. Miyano
Department of Physics, Brooklyn College, Brooklyn, New York 11210, USA

W. E. Spicer
Department of Electrical Engineering, Stanford University, Stanford, California 94305, USA

The relaxation of the surface P atoms, for both the clean and Bi-covered GaP(110) surface, was studied with x-ray standing wave (XSW) spectroscopy using surface-sensitive x-ray photoelectron as the XSW modulated signal. The photoemission signal of the outermost surface layer is mixed with the signal from the remaining near surface of the underlying substrate, so further analysis is required to calculate the geometry of the relaxation of the surface atoms. We present a general analysis method for extracting the geometry of the surface reconstruction that minimizes the propagation of the uncertainties associated with fitting XSW data. It takes advantage of the fact that the coherent distance may be more accurately determined than the coherent fraction in XSW data analysis. This method makes use of the electron attenuation length, and shows that the relaxation is only weakly dependent on the uncertainties of this parameter. Results indicate that, for the clean GaP surface, P relaxes with a small outward rotational displacement, with the axis of the rotation located at the second-layer Ga site, whereas, for the Bi-covered case, relaxation consists of a rotation in the opposite direction. The magnitude of the contraction is not negligible, and might be important in the interpretation of low-energy electron diffraction data and in *ab initio* calculations.

I. INTRODUCTION

X-ray standing wave (XSW) spectroscopy has been widely employed in the study of the absorbent sites of adatoms.[1–3] It has also been successfully applied to both clean[4] and covered[5–7] surface relaxation. XSW relies on the fact that when an x-ray impinges on a crystalline substrate near a Bragg condition, the incident beam is strongly reflected, and the superposition of the incident and reflected beams forms an x-ray standing wave that has the periodicity of the reflecting Bragg planes of the crystal lattice. The intensity of the electric field is no longer uniform throughout the crystalline unit cell, but depends strongly on the crystallographic position and on the phase of the standing wave. Because the photoelectron emission from an atom is proportional to the electric-field intensity at the position of its core (dipole approximation), the XSW yield (Y) from an atom under XSW excitation obeys the following relation:[8]

$$Y_{\mathbf{H}}(E,\theta) \sim 1 + R_{\mathbf{H}}(E,\theta)$$
$$+ 2f_c^{\mathbf{H}}\sqrt{R_{\mathbf{H}}(E,\theta)}\cos\left[\nu_{\mathbf{H}}(E,\theta) - 2\pi\frac{D_c^{\mathbf{H}}}{d_{\mathbf{H}}}\right], \quad (1)$$

where $\mathbf{H}$ is the crystal vector of the reflecting Bragg planes,

$\nu_{\mathbf{H}}$ is the phase difference between the incident and reflected beams, $R_{\mathbf{H}}$ is the intensity of the reflected beam [the latter two are both functions of the energy (E) and angle (θ) of the incident beam][8,9] and $d_{\mathbf{H}} \equiv 1/|\mathbf{H}|$ is the interplanar distance. The structural information is contained in the coherent distance ($D_c^{\mathbf{H}}$) and coherent fraction ($f_c^{\mathbf{H}}$), which are structural parameters that can be extracted from the XSW spectra. They are defined as the phase and amplitude of the Fourier integral of the distribution function $P_{\mathbf{H}}(D)$ over an interplanar distance, with wave vector equal to the Bragg plane vector, as follows:

$$\int_0^{d_{\mathbf{H}}} dD P_{\mathbf{H}}(D)\exp\left(-2\pi i\frac{D}{d_{\mathbf{H}}}\right) = f_c^{\mathbf{H}}\exp\left(-2\pi i\frac{D_c^{\mathbf{H}}}{d_{\mathbf{H}}}\right), \quad (2)$$

where D is the perpendicular distance to the closest atomic plane (i.e., parallel to $\mathbf{H}$), and the product $P_{\mathbf{H}}(D)dD$ is the fraction of atoms that reside between D and $D+dD$. The normalized coherent distance $D_c^{\mathbf{H}}/d_{\mathbf{H}}$ can be viewed as an "averaged" distance in units of the interplanar spacing, so it can take values between −0.5 and 0.5. The periodicity of the XSW electric field is equal to the interplanar distance of the reflecting planes. The coherent fraction then depends on the spread of positions taken by the atoms of interest in the in-

terplanar period; its value is maximum (equal to 1) when the distribution function is sharp, i.e., when all atoms take equivalent positions; its value is minimum (zero) when the atomic distribution is constant between the crystal planes. In principle, it is possible to reconstruct the distribution function in real space from a large enough number of reflections (**H**), allowing the back transform of Eq. (2).[10] For less complex systems, such as the subject of the present study, it is possible to model the distribution function in terms of a finite and small number of parameters, such as the coordinates of the atomic sites. This allows for the determination of the geometry with a finite number of Bragg reflections.

In our study, the XSW yield from the P atoms at the GaP(110) surface was obtained by collecting the P 1s photoelectron emission. The intensity of the P 1s core line does not arise exclusively from the P surface atoms of interest but also from the P atoms that reside in the near surface region, so $D_c^{\mathbf{H}}$ appears as an attenuation-length-weighted average (see Sec. III C) of the position of the relaxed outermost layer, the second layer, and so on. The value of $f_c^{\mathbf{H}}$ reflects the diversity of these positions.[11] Surface relaxation studies therefore require the use of surface-sensitive photoemission or Auger electron emission that contains an appreciable contribution ($\geq 30\%$) from the outermost layer. To extract the atomic geometry of the outermost layer from $f_c^{\mathbf{H}}$ and $D_c^{\mathbf{H}}$, it is necessary to assume that the remaining layers, excluding the outermost surface layer, from the second layer on, assume positions that do not deviate significantly from their ideal bulk sites. This assumption is expected to be a good approximation for surfaces such as the GaP(110) 1×1 surface that exhibits only a relaxation rather than a reconstruction. Because the surface atomic position is reflected in both $f_c^{\mathbf{H}}$ and $D_c^{\mathbf{H}}$, it carries with it the uncertainties associated with these parameters. Here, we use a method that avoids modeling $f_c^{\mathbf{H}}$ because the uncertainties associated with $f_c^{\mathbf{H}}$ are typically much larger than those for $D_c^{\mathbf{H}}$, even in standard XSW modeling. Woicik *et al.* solved the surface relaxation of InP(110) with an analysis method that also minimized the effect of $f_c^{\mathbf{H}}$.[4]

In the current experiments, we employ core-level photoemission as the XSW modulated data. Because the elastic photoemission intensity arises solely from the direct photoexcitation caused by the x-ray standing wave field, it is possible to impose consistency with electron attenuation-length information. In Sec. III, we present an analysis method that employs the known values of the electron attenuation length for GaP, which in addition has the advantage that the final result is not very sensitive to uncertainties in these values. We performed experiments to measure the relaxation of phosphorus atoms for clean and bismuth-covered GaP(110) surfaces. The method we employed was particularly suitable for substrate relaxation studies because the results were not affected by the presence of thin overlayers, so clean and overlayer-covered surfaces can be unambiguously compared. This is not the case with other techniques, such as low-energy electron diffraction (LEED), which are significantly more model dependent. We used reflections from three Bragg conditions to triangulate the position of phosphorus in space. A XSW triangulation study of the sitting position of bismuth

on GaP(110) has been reported elsewhere.[12] Our results are consistent with the epitaxial-continued layer structure (ECLS) for group-V overlayer structure on III-V (110) surfaces.[13]

II. EXPERIMENTS AND RESULTS

A. Experiment details

XSW experiments were performed utilizing the (200), (111), and (11$\bar{1}$) reflections of GaP(110) on beamline 3-3 at the Stanford Synchrotron Radiation Laboratory. The photon energy was scanned across the Bragg condition with a double crystal Si (111) monochromator. Phosphorus XSW data were recorded by monitoring the photoemission intensity of the P 1s core level and the *KLL* Auger line with a cylindrical mirror analyzer (CMA). Because both the core level and Auger peaks ride on top of a background of inelastically scattered electrons, background XSW data were also recorded and subtracted from the on-peak data. We also simultaneously and independently recorded the reflectivity ($R_{\mathbf{H}}$) and total photoelectron yield ($Y_{\mathbf{H}}^T$). The $Y_{\mathbf{H}}^T$ was recorded by monitoring the total current leaving the sample. The ultrahigh-vacuum systems had base pressures in the low 10^{-8} Pa range. The chamber manipulator had one angular and three linear degrees of freedom. Clean surfaces were prepared by cleaving outgassed GaP crystals along the (110) face. All cleaves were mirrorlike. Bismuth-covered surfaces were prepared by evaporating approximately one monolayer of Bi as measured by a quartz crystal oscillator, and annealed at 325 °C for 10 min to desorb any Bi in excess of one monolayer and to further enhance the interfacial order.[14] For the (200) reflection, the sample surface was at 45° from the incoming beam, while for the (111) and (11$\bar{1}$) reflections, the sample surface was facing the beam. In all cases, the (001) crystallographic direction pointed vertically.

Many peak and background data were recorded in order to achieve good statistics. The files were then added or subtracted depending on whether they correspond to the peak or to the background. The photon energy slightly shifted with time due to the cooling of the monochromator crystals with decaying stored beam current. The spectra were aligned in energy by maximizing the correlation between the measured reflectivity curve of the different files prior to addition (or subtraction). For the sample orientation used for the (111) and (11$\bar{1}$) reflections, the (111) diffracting planes of the Si crystals in the monochromator were nearly parallel to the GaP(111) [or (11$\bar{1}$)] Bragg planes.[1] While not entirely nondispersive, this configuration provided better resolution than the (200) reflection, which was acquired through back-reflection geometry.[15]

B. Results

The experiments performed are listed in Table I. The P *KLL* and P 1s data were taken for the same surfaces and under identical conditions. Figure 1 shows the P 1s XSW data for the clean and Bi-covered surfaces (see Table I) together with their best fits. The quality of each fit is represen-

TABLE I. Experiments performed and fitting results. Also displayed are the final kinetic energy of the P $1s$ photoelectrons as well as the corresponding effective attenuation length (EAL).

			Clean surface		Bismuth covered	
			P *KLL*	P $1s$	P *KLL*	P $1s$
(200)	Sample 1	D_c	0.019	0.023		
		f_c	0.86	0.87		
		E_K, EAL	1850 eV, 32 Å	125 eV, 4.3 Å		
	Sample 2	D_c	0.016	0.024		
		f_c	0.88	0.90		
		E_K, EAL	1850 eV, 32 Å	125 eV, 4.3 Å		
	Sample 3	D_c	0.007	0.019	−0.005	−0.02
		f_c	0.81	0.83	0.86	0.84
		E_K, EAL	1850 eV, 32 Å	125 eV, 4.3 Å	1850 eV, 32 Å	125 eV, 4.3 Å
(111)	Sample 1	D_c	0.001	0.004		−0.008
		f_c	1	0.99		0.97
		E_K, EAL	1850 eV, 32 Å	170 eV, 5 Å		170 eV, 5 Å
	Sample 2	D_c	0.001	0.003		
		f_c	1	1.01		
		E_K, EAL	1850 eV, 32 Å	170 eV, 5 Å		
(11$\bar{1}$)	Sample 4	D_c	−0.004	0.008		
		f_c	0.94	0.934		
		E_K, EAL	1850 eV, 32 Å	165 eV, 5 Å		

tative of the quality for all surfaces studied. The reflectivity, which provides fiducial information on the energy calibration, energy resolution, and properties of the incident x-ray beam, is also plotted with the data. The fittings were done with AXSWA,[16] a software that employs a deconvolution method to subtract the characteristic effects of the incident x-ray beam from the shape of the XSW signal.[17] The extracted values for the coherent distance and coherent fraction for all the reflections performed are also displayed in Table I. The coherent distances are in units of the corresponding interplanar distance. The origin was chosen as the location of the crystallographic P site. The x-ray atomic structure factors were obtained utilizing the softwares ABS (Ref. [18]) and XOP (Ref. [19]).

As shown in Table I, the values of the coherent fraction corresponding to P $1s$ and *P KLL* were similar in each case. This suggested that the nondipole photoemission effects were not significant. These effects are small in general, and were further reduced due to the angular integration of the CMA and the low energy (<2.5 keV) of the x rays employed in each experiment.[20–22]

The photon energy of the incoming beam was chosen to maintain the kinetic energy of P $1s$ photoelectrons lying in the 50–200 eV range. In this way, the attenuation length of the outcoming P $1s$ photoelectrons is minimized.[23] As shown in Sec. III B, for the range of electron energies mentioned, the contribution to the photoemission peak signal from the atoms located in the outermost layer is appreciable [~58% for the (200) configuration and ~60% for the (111) and

(11$\bar{1}$) configurations]. The remaining signal comes from atoms located beneath the first surface layer, i.e., in the near surface. No surface-sensitive core level was available for Ga for the photon energies used in the experiments, so the Ga relaxation was not determined.

Phosphorus bulk sensitive data (*KLL* Auger line) were also collected. As shown in the following section, systematic errors in the data analysis could be eliminated by comparing the two sets of data, one containing information on the surface relaxation, and the other from atoms at the remaining bulk positions. The effective attenuation length for P *KLL* electrons (1850 eV) is ~32 Å,[24] so the contribution of the outermost layer to the total signal is on the order of 15%.

C. Compared coherent distances between the P $1s$ and P *KLL* data

The analysis results for the coherent distances for the P $1s$ experiments were close to zero (see Table I), which alone implies small relaxation; however, the P $1s$ coherent distances were consistently larger than the coherent distance of P *KLL* for the clean surface. The opposite was observed for the P $1s$ coherent distances in the presence of the Bi overlayer, which were consistently smaller than those corresponding to P *KLL*. This implied expansion in the clean surface case, and contraction in the Bi-covered case.

Errors in the values used for the structure factors may introduce errors comparable to the deviations of the P *KLL* coherent distance from zero. Notice that the photon energy is
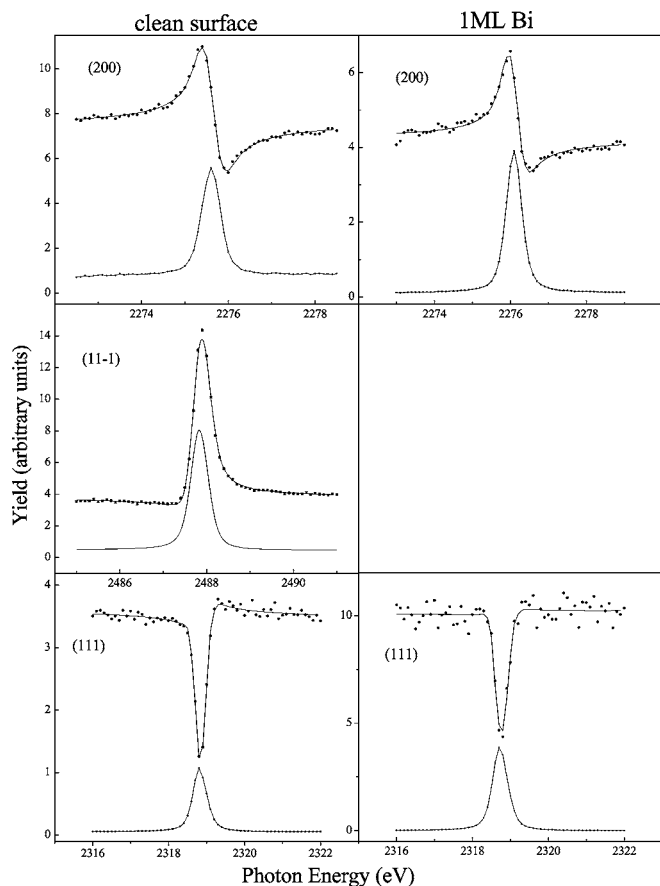
FIG. 1. P 1 *s* XSW data and theoretical fit for the (200) reflection for a clean surface (sample 1). The bottom curve is the reflectivity.

within 200 eV of the P 1*s* edge. The atomic structure factors are strong functions of energy near an absorption edge and are therefore theoretically less reliable. The difference between the coherent distance of the P 1*s* measurements and the coherent distance of the P *KLL* measurements was believed to help better avoid systematic errors. The differences were small, but still detectable by eye in the raw XSW data (see Fig. 2). The software AXSWA allows for a direct determination of the difference in $D_c^{\mathbf{H}}$ by simultaneously fitting the spectra for P 1*s* and P *KLL*.[16] The difference between the
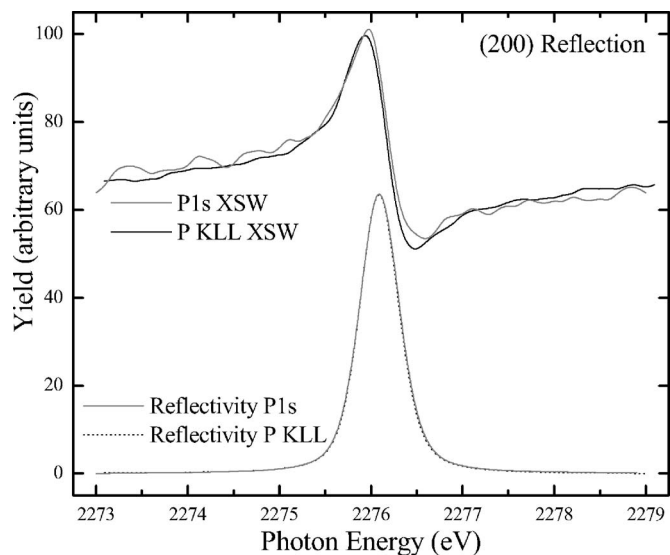

FIG. 2. Comparison between the P 1 *s* and P *KLL* XSW signals. The shift, although small, was visible from the rough data. The experimental reflectivity curves were stacked one on top of the other.

coherent distances of the two sets of data was one of the free parameters, while the other related free parameter was the average. The results of the analysis are summarized in Table II.

The uncertainty of the corrected coherent distance was assessed from the level of reproducibility of the results, and is displayed in the column for the averaged values in Table II. For the experiments that were done once, the uncertainty was chosen as the largest value. As shown in Sec III A, the values of the coherent fraction were not employed in the relaxation calculations.

III. ANALYSIS AND DISCUSSION

A. Modeling the distribution function and solving for the geometrical parameters

The position of bulk atoms in perfect crystals is periodic, holding positions corresponding to the perfect lattice perturbed only by temperature vibrations. The termination of a

TABLE II. Differences in the coherent distance ($D_c^{\mathbf{H}}$) between the P 1*s* and P *KLL* XSW data in interplanar units. The last column shows the results for $D_S^{\mathbf{H}}$ obtained through Eq. (8).

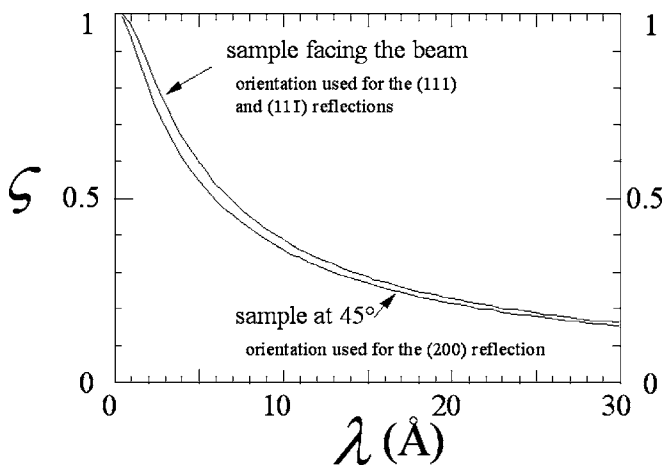|	**H**	$(D_c^{\mathrm{P}\ 1s}-D_c^{\mathrm{P}\ KLL})/d_{\mathbf{H}}$	Averaged	$D_S^{\mathbf{H}}/d_{\mathbf{H}}$
Clean surface	(200) 1	+0.004		
	(200) 2	+0.008	+0.008±0.004	+0.019±0.009
	(200) 3	+0.012		
	(111) 1	+0.0025	+0.002±0.001	+0.005±0.002
	(111) 2	+0.0022		
	(11$\bar{1}$) 4	+0.012	+0.012±0.004	+0.026±0.009
With Bi	(200) 3	−0.015	−0.015±0.004	−0.035±0.008
	(111) 1	−0.008	−0.008±0.004	−0.017±0.008

FIG. 3. Fraction of the signal coming from the outermost substrate layer as a function of escape depth. The calculations were done by integrating Eq. (7) for the angle acceptance of the CMA, for each of the sample orientations corresponding to the different reflections.

crystal induces relaxation, which is larger for the substrate layers closer to the surface. The complete determination of this relaxation, and how it is changed by the presence of an overlayer, is an extremely difficult and important problem. In this analysis, it was considered that only the last substrate layer deviates from the ideal lattice positions, an assumption that is supported by LEED studies.[25] As mentioned earlier, the LEED pattern for both the clean and Bi-covered GaP surface held a (1×1) symmetry, implying that the deformation was only a relaxation of the surface atoms. Thus, the problem was reduced to finding the relaxation coordinates of the surface (1×1) unit cell.

Because the P $1s$ signal recorded had contributions from P at the surface layer ($\sim 60\%$) and from the rest of the P in the crystal ($\sim 40\%$), two positions—the relaxed outermost surface layer and the bulk—were considered in the distribution function. Ignoring thermal vibrations, the distribution function can be written as follows:

$$P_{\mathbf{H}}(D) = \zeta\delta(D - D_S^{\mathbf{H}}) + (1 - \zeta)\delta(D - D_B^{\mathbf{H}}), \quad (3)$$

where ζ is the fraction of the signal coming from the outermost P atoms, and $D_S^{\mathbf{H}}$ and $D_B^{\mathbf{H}}$ are the distances of the surface and bulk atoms from the local Bragg planes. Because the bulk P position $D_B^{\mathbf{H}}$ is known (equal to zero), the problem was reduced to finding $D_S^{\mathbf{H}}$. This was done independently for the (200), (111), and (11$\bar{1}$) Bragg reflections. These three vectors are noncoplanar, so it was possible to triangulate in space the coordinates of the relaxed surface atoms.

The parameters of the distribution function [Eq. (3)] are related to the coherent distance and coherent fraction by Eq. (2). By performing the integrals, we obtain

$$f_c^{\mathbf{H}} = \left| (1 - \zeta)\exp\left(-2\pi i\frac{D_B^{\mathbf{H}}}{d_{\mathbf{H}}}\right) + \zeta\exp\left(-2\pi i\frac{D_S^{\mathbf{H}}}{d_{\mathbf{H}}}\right) \right|, \quad (4)$$
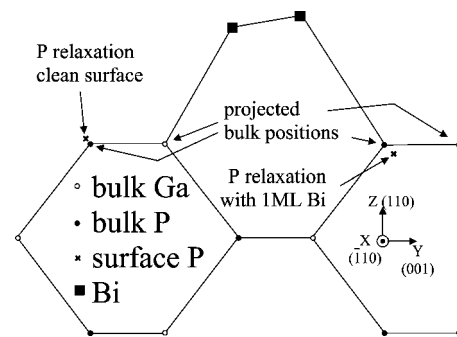
and

FIG. 4. Relaxation of the outermost P atoms for the clean and Bi-covered (110) GaP surface scaled to our results. Also included is the previously reported geometry of the Bi adatoms (see Ref. 12). For visualization, the projected bulk positions close to the relaxed positions are also drawn.

$$D_c^{\mathbf{H}} = \frac{d_{\mathbf{H}}}{2\pi} \arctan \frac{(1 - \zeta)\sin\left(2\pi\frac{D_B^{\mathbf{H}}}{d_{\mathbf{H}}}\right) + \zeta\sin\left(2\pi\frac{D_S^{\mathbf{H}}}{d_{\mathbf{H}}}\right)}{(1 - \zeta)\cos\left(2\pi\frac{D_B^{\mathbf{H}}}{d_{\mathbf{H}}}\right) + \zeta\cos\left(2\pi\frac{D_S^{\mathbf{H}}}{d_{\mathbf{H}}}\right)}. \quad (5)$$

Equations (4) and (5) comprise a complete set for each reflection $\mathbf{H}$, and can be inverted to obtain the values of ζ and $D_S^{\mathbf{H}}$ from the experimental values of the coherent fraction ($f_c^{\mathbf{H}}$) and coherent distance ($D_c^{\mathbf{H}}$). However, as mentioned in the Introduction, we avoided employing the $f_c^{\mathbf{H}}$ because of its larger uncertainty. An alternative method was to estimate ζ using tabulated values of the escape depth. There is extensive literature about the escape depth of electrons as a function of kinetic energy.[24,26] Equation (5) involves the coherent distance $D_c^{\mathbf{H}}$, but not the coherent fraction $f_c^{\mathbf{H}}$. By evaluating ζ using electron attenuation-length information, it is possible to avoid the use of Eq. (4). In this way, the use of $f_c^{\mathbf{H}}$ was avoided in the determination of the atomic surface reconstruction.

B. Fraction of the photoemission signal coming from the outermost P atoms

The elastic P $1s$ photoelectron peak corresponds to P $1s$ core electrons that have not lost energy by electron-electron collisions. It was shown by Spicer that the probability of escape without electron-electron collisions (P_E) of a photoelectron generated at position $\mathbf{r}$ and excited with energy E is expressed as follows[27]:

$$P_E(\mathbf{r}) = \exp\left(-\frac{\mathbf{r} \cdot \mathbf{n}}{\lambda(E)\cos\theta}\right),$$

where θ is the detection angle normal to the crystal surface ($\mathbf{n} = 1/\sqrt{8}[220]$), and λ is the attenuation length. The origin was set at the surface to make $\mathbf{r} \cdot \mathbf{n}$ the distance from the

generation of the photoelectron to the surface. The fraction of surface signal $\varsigma(E,\theta)$ is then given by

$$\zeta(E,\theta) \equiv \frac{\text{surface signal}}{\text{total signal}} = 1 - \exp\left(\frac{d_{[220]}}{\lambda(E)\cos\theta}\right), \quad (6)$$

where $d_{[220]}$ is the distance between the atomic planes parallel to the sample surface. As shown by Lindau and Spicer, for most materials (GaP included) the escape length of electrons with energy between 50 and 200 eV is between 4 and 10 Å, so a considerable fraction of the signal arises from the outermost layer.[26] An important point is that Eq. (6) is valid whether or not the substrate surface is covered by an overlayer, so a meaningful comparison can be done between the clean and Bi-covered surfaces. Equation (6) was integrated for the angle of acceptance of the CMA ($42.3° \pm 6°$) for the sample orientations used in the nondispersive configuration—where the sample faced the beam—and for the orientation used for the (200) reflection—where the sample makes a 45° angle with the incoming beam. The integration was calculated as follows:

$$\zeta \equiv \overline{\zeta(E,\theta)} = \frac{\int d\Omega \left[1 - \exp\left(-\frac{d_{[220]}}{\lambda(E)\cos\theta}\right) \right]}{\int d\Omega}. \quad (7)$$

It can be seen in Fig. 3 that the surface sensitivity ζ for the sample orientations corresponding to the three reflections [which were calculated using Eq. (7)] are very close to each other for all values of the attenuation length λ. There has been enormous progress in the determination of the attenuation length, and effective attenuation lengths are provided that account for inelastic as well as for elastic scattering through the Monte Carlo method. The employed values, which were determined using Ref. 24, are depicted in Table I. From the curves of Fig. 3, the corresponding values for ζ are 0.58 [P $1s$ (200) reflection], 0.6 [P $1s$ (111) and $(11\bar{1})$ reflections], and 0.15 (all P *KLL*). From the flat slope of the curves in Fig. 3, uncertainties in the attenuation length introduced small uncertainties in ζ, and did not contribute significantly to the overall uncertainty.

C. Determination of the relaxation coordinates

Equation (5) provides the dependence of $(D_c^{\text{P }1s} - D_c^{\text{P }KLL})/d_{\textbf{H}}$ on $D_S^{\textbf{H}}$. This can be directly seen by rearranging that equation as follows (with $D_B^{\textbf{H}}$ set to zero):

$$\frac{D_{c,\text{P }1s}^{\textbf{H}}}{d_{\textbf{H}}} - \frac{D_{c,PKLL}^{\textbf{H}}}{d_{\textbf{H}}} = \frac{1}{2\pi}\arctan\frac{\zeta_{\text{P }1s}\sin\left(2\pi\frac{D_S^{\textbf{H}}}{d_{\textbf{H}}}\right)}{(1-\zeta_{\text{P }1s}) + \zeta_{\text{P }1s}\cos\left(2\pi\frac{D_S^{\textbf{H}}}{d_{\textbf{H}}}\right)} - \frac{1}{2\pi}\arctan\frac{\zeta_{PKLL}\sin\left(2\pi\frac{D_S^{\textbf{H}}}{d_{\textbf{H}}}\right)}{(1-\zeta_{PKLL}) + \zeta_{PKLL}\cos\left(2\pi\frac{D_S^{\textbf{H}}}{d_{\textbf{H}}}\right)}. \quad (8)$$

Equation (8) was employed to calculate the values of $D_S^{\textbf{H}}$ depicted in Table II. A generous range for ζ would not introduce significant uncertainty in $D_S^{\textbf{H}}$. Therefore, the most important contribution to the uncertainty in the value of $D_S^{\textbf{H}}$ came from the uncertainty in $D_c^{\text{P }1s} - D_c^{\text{P }KLL}$.

The coordinates of the relaxation can be obtained by triangulating the results of $D_S^{\textbf{H}}$. The coordinates of the reconstruction, as defined in Fig. 4, depend on $D_S^{\textbf{H}}$ as follows:

$$X = \left(\frac{D_S^{(111)}/d_{(111)} + D_S^{(11\bar{1})}/d_{(11\bar{1})}}{\sqrt{8}} - \frac{D_S^{(200)}/d_{(200)}}{2} \right) a_l,$$

$$Y = \frac{D_S^{(111)}/d_{(111)} - D_S^{(11\bar{1})}/d_{(11\bar{1})}}{2} a_l, \quad (9)$$

$$Z = \frac{D_S^{(111)}/d_{(111)} + D_S^{(11\bar{1})}/d_{(11\bar{1})}}{\sqrt{8}} a_l,$$

where a_l is the lattice constant. For the clean surface, all three reflections were performed and the three coordinates of

the phosphorus reconstruction could be directly obtained from Eqs. (9), and are displayed in Table III. It was reassuring that the value for X was within 0.01 Å from the expected value of zero [the (1×1) LEED symmetry is consistent with a zero relaxation or with two equivalent opposite displacements that would anyway average to zero].

The $(11\bar{1})$ reflection was not performed for the Bi-covered surface. However, it was possible to solve Eqs. (9) by assuming a zero displacement in the $(\bar{1}10)$ direction ($X=0$). The results are shown in Table III. Figure 4 shows the P relaxation scaled to our results. For the clean surface, the relaxation is a small counterclockwise rotation, while for the covered surface, it is a rotation in the opposite direction. Also included are the positions of the Bi atoms. They were determined previously in a related work.[12] There are not theoretical results for the Bi/GaP system; however, the result is consistent with theoretical calculations of the ECLS model of a monolayer of Bi in other III-V (110) surfaces.[28]

The magnitude of the contraction of the P outermost atoms induced by the presence of Bi was not negligible (about 0.2 Å deeper than for the clean surface, see Fig. 4). This

TABLE III. Relaxation of P (from the ideal position) determined by this study. Results from other studies are also shown.

Distance	Clean surface			With Bi
(Å)	XSW	LEED	FPP	XSW
$(\bar{1}10)$ X	0.01 ± 0.04	0 (assumed)	0 (assumed)	0 (assumed)
(001) Y	-0.06 ± 0.03	-0.31	0	0.1 ± 0.09
(110) Z	0.06 ± 0.02	0.09	0	-0.13 ± 0.03

might be of importance to the calculations performed to interpret LEED measurements, as well as *ab initio* calculations. The capability of measuring such contraction directly is unique to XSW.

D. Comparison to other techniques

Also displayed in Table III are the results from LEED experiments[25] and first-principles pseudopotential (FPP) calculations[29] for the relaxation of P for the clean GaP(110) surface. No comparison could be made for the covered surface. In comparing with other techniques, it should be kept in mind that the XSW technique is sensitive to the displacement of the surface atoms relative to the ideal crystal lattice, and other techniques might be more sensitive to displacements relative to the previous layer. Both LEED and FPP papers reported the relaxation results in terms of the relative distance between the atoms and between the layers. Those results had to be transformed into absolute displacements to be compared to the XSW results. Both works assumed a zero displacement in the $(\bar{1}10)$ direction.

The XSW results compare to the LEED results for the displacement perpendicular to the surface (Z), although the agreement is not as good for the displacement parallel to the surface (Y).

IV. CONCLUSIONS

The relaxation of surface P atoms for the clean GaP(110) surface, as well as in the presence of a Bi overlayer, was triangulated by the XSW technique using surface-sensitive electron detection. The method presented for measuring the position of P surface atoms for the clean GaP(110) surface was directly applied to the Bi-covered surface, so the effect of the Bi overlayer on the substrate relaxation could be unambiguously determined. For the clean surface, the P relaxation was a small outward rotation with its axis centered at the position of the second-layer Ga atom. The effect of the Bi overlayer on the P relaxation was a small inward rotation.

[1] D. P. Woodruff, Rep. Prog. Phys. **68**, 743 (2005).

[2] J. Zagenhagen, Surf. Sci. Rep. **18**, 199 (1993).

[3] A. Herrera-Gómez, P. Pianetta, D. Marshall, E. Nelson, and W. E. Spicer, Phys. Rev. B **61**, 12988 (2000); G. E. Franklin, S. Tang, J. C. Woicik, M. J. Bedzyk, A. J. Freeman, and J. A. Golovchenko, *ibid.* **52**, R5515 (1995); G. E. Franklin, M. J. Bedzyk, J. C. Woicik, C. Liu, J. R. Patel, and J. A. Golovchenko, *ibid.* **51**, 2440 (1995).

[4] J. C. Woicik, T. Kendelewicz, K. E. Miyano, P. L. Cowan, C. E. Bouldin, B. A. Karlin, P. Pianetta, and W. E. Spicer, Phys. Rev. Lett. **68**, 341 (1992).

[5] J. R. Patel, D. W. Berreman, F. Sette, P. H. Citrin, J. E. Rowe, P. L. Cowan, T. Jach, and B. Karlin, Phys. Rev. B **40**, 1330 (1989).

[6] J. C. Woicik, T. Kendelewicz, A. Herrera-Gómez, K. E. Miyano, P. L. Cowan, C. E. Bouldin, P. Pianetta, and W. E. Spicer, Phys. Rev. Lett. **71**, 1204 (1993).

[7] J. C. Woicik, T. Kendelewicz, S. A. Yoshikawa, K. E. Miyano, G. S. Herman, P. L. Cowan, P. Pianetta, and W. E. Spicer, Phys. Rev. B **53**, 15425 (1996).

[8] D. P. Woodruff, D. L. Seymour, C. F. McConville, C. E. Riley, M. D. Crapper, and N. P. Prince, Surf. Sci. **195**, 237 (1988).

[9] A. Herrera-Gómez, Ph.D. thesis, Stanford University, 1994; SLAC Report No. 438, 1994 (unpublished).

[10] L. Cheng, P. Fenter, M. J. Bedzyk, and N. C. Sturchio, Phys. Rev. Lett. **90**, 255503 (2003).

[11] The outermost surface layer is chemically shifted from the rest of the substrate atoms, and could be discriminated from photoemission signal. With high-resolution PES data obtained as a function of the XSW phase, it could be possible to perform surface relaxation studies in a more direct way than in the present study. However, those experiments would require x-ray beams with dispersion on the order of a few tenths of an eV to carry out such chemical discrimination.

[12] A. Herrera-Gómez, T. Kendelewicz, J. C. Woicik, K. E. Miyano, P. Pianetta, S. Southworth, P. L. Cowan, B. A. Karlin, and W. E. Spicer, J. Vac. Sci. Technol. A **12**, 2473 (1994).

[13] A. Umerski and G. P. Srivastava, Phys. Rev. B **51**, 2334 (1995).

[14] F. Schaffler, R. Ludeke, A. Taleb-Ibrahimi, G. Hughes, and D. Rieger, J. Vac. Sci. Technol. B **5**, 1048 (1987).

[15] K. E. Miyano, T. Kendelewicz, J. C. Woicik, P. L. Cowan, C. E. Bouldin, B. A. Karlin, P. Pianetta, and W. E. Spicer, Phys. Rev. B **46**, 6869 (1992).

[16] The software AXSWA allows for the simultaneous fitting of two sets of data, which is important for comparison purposes. It can also directly assess the uncertainty of the difference in the parameter values between the two sets of data. Another feature of AXSWA is that it can account for an arbitrary energy dispersion of the incident beam through a deconvolution process; a copy of the program can be obtained at http://qro.cinvestav.mx/~aherrera/xsw_software

[17] A. Herrera-Gómez, P. M. Rousseau, T. Kendelewicz, J. C. Woicik, J. Plummer, and W. E. Spicer, J. Appl. Phys. **85**, 1429 (1999).

[18] S. Brennan and P. L. Cowan, Rev. Sci. Instrum. **63**, 850 (1992).

[19] M. Sanchez del Rio and R. J. Dejus, Proc. SPIE **2448**, 340 (1998).

[20] C. J. Fishery, R. Ithiny, R. G. Jonesy, G. J. Jacksonz, D. P. Woodruffz, and B. C. C. Cowiex, J. Phys.: Condens. Matter **10**, L623 (1998).

[21] E. J. Nelson, J. C. Woicik, P. Pianetta, I. A. Vartanyants, and J. W.

Cooper, Phys. Rev. B **65**, 165219 (2002).

[22] G. J. Jackson, B. C. C. Cowie, D. P. Woodruff, R. G. Jones, M. S. Kariapper, C. Fisher, A. S. Y. Chan, and M. Butterfield, Phys. Rev. Lett. **84**, 2346 (2000).

[23] W. E. Spicer and F. Wooten, Proc. IEEE **51**, 1119 (1963).

[24] C. J. Powell and A. Jablonski, NIST Standard Reference Database 82, Version 1.0, 2001.

[25] C. B. Duke, A. Paton, W. K. Ford, A. Kahn, and J. Carelli, Phys. Rev. B **24**, 562 (1981).

[26] I. Lindau, and W. E. Spicer, J. Electron Spectrosc. Relat. Phenom. **3**, 409 (1974).

[27] W. E. Spicer, Phys. Rev. **112**, 114 (1958).

[28] A. Umerski and G. P. Srivastava, Phys. Rev. B **51**, 2334 (1995).

[29] G. P. Srivastava, J. Phys.: Condens. Matter **5**, 4695 (1993).